Angle-gather time migration

Sergey Fomel and Marie Prucha

sergey@sep.stanford.edu, marie@sep.stanford.edu

ABSTRACT

Angle-gather migration creates seismic images for different reflection angles at the reflector. We formulate an angle-gather time migration algorithm and study its properties. The algorithm serves as an educational introduction to the angle gather concept. It also looks attractive as a practical alternative to conventional common-offset time migration both for velocity analysis and for AVO/AVA analysis.

1. Introduction

Angle-gather migration creates seismic images collected by the reflection angle at the point of reflection. Major advantages of this approach are apparent in the case of prestack depth migration. As shown by Prucha et al. (1999), the ray pattern of angle-gather migration is significantly different from that of the conventional common-offset migration. The difference can be exploited for overcoming illumination difficulties of the conventional depth migration in complex geological areas.

In this paper, we explore the angle-gather concept in the case of prestack time migration. The first goal of this study is educational. Since we can develop the complete mathematical theory of angle-gather time migration analytically, it is much easier to understand the most basic properties of the method in the time migration domain. The second goal is practical. Angle gathers present an attractive tool for post-migration AVO/AVA studies and velocity analysis, and even the most basic time migration approach can find a valuable place in the complete toolbox of seismic imaging.

We start with analyzing the traveltime relations for the basic Kirchhoff implementation of angle-gather time migration. The analysis follows

Fowler's general approach to prestack time migration methods (Fowler, 1997). Next, we derive formulas for the amplitude weighting and discuss some frequency-domain approaches to angle gathers. Finally, we present simple synthetic tests of the method and discuss further research directions.

2. Traveltime considerations

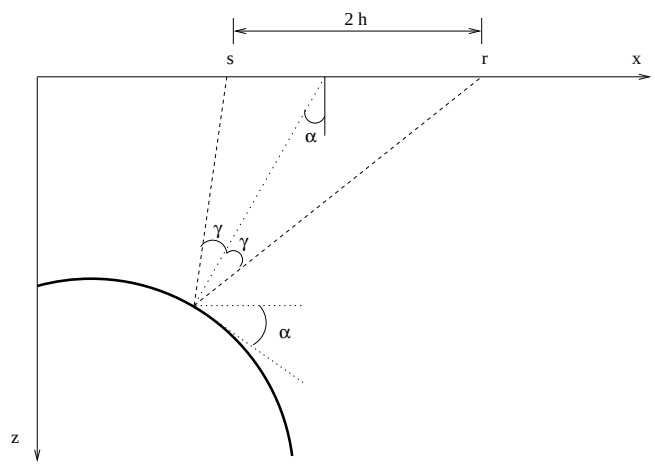

Figure 1: Reflection rays in a constant-velocity medium: a scheme. rays [NR]

Let us consider a simple reflection experiment in an effectively constant-velocity medium, as depicted in Figure 1. The pair of incident and reflected

rays and the line between the source s and the receiver r form a triangle in space. From the trigonometry of that triangle we can derive simple relationships among all the variables of the experiment (Fomel, 1995, 1996a, 1997).

Introducing the dip angle α and the reflection angle γ, the total reflection traveltime t can be expressed from the law of sines as

$$t = \frac{2h}{v}\,\frac{\cos(\alpha+\gamma)+\cos(\alpha-\gamma)}{\sin 2\gamma} = \frac{2h}{v}\,\frac{\cos\alpha}{\sin\gamma}\;, \tag{1}$$

where v is the medium velocity, and h is the half-offset between the source and the receiver.

Additionally, by following simple trigonometry, we can connect the half-offset h with the depth of the reflection point z, as follows:

$$h = \frac{z}{2}\,\frac{\sin 2\gamma}{2\cos(\alpha+\gamma)\cos(\alpha-\gamma)} = z\,\frac{\sin\gamma\,\cos\gamma}{\cos^2\alpha-\sin^2\gamma}\;. \tag{2}$$

Finally, the horizontal distance between the midpoint x and the reflec-

tion point ξ is

$$x-\xi = h\,\frac{\cos(\alpha-\gamma)\sin(\alpha+\gamma)+\cos(\alpha+\gamma)\sin(\alpha-\gamma)}{\sin 2\gamma} = h\,\frac{\sin\alpha\,\cos\alpha}{\sin\gamma\,\cos\gamma} \tag{3}$$

Equations (1–3) completely define the kinematics of angle-gather migration. Regrouping the terms, we can rewrite the three equations in a more symmetric form:

$$t = \frac{2z}{v}\,\frac{\cos\alpha\,\cos\gamma}{\cos^2\alpha-\sin^2\gamma} \tag{4}$$

$$h = z\,\frac{\sin\gamma\,\cos\gamma}{\cos^2\alpha-\sin^2\gamma} \tag{5}$$

$$x-\xi = z\,\frac{\sin\alpha\,\cos\alpha}{\cos^2\alpha-\sin^2\gamma} \tag{6}$$

For completeness, here is the inverse transformation from t, h, and $x-\xi$ to

z, γ, and α:

$$z^2 = \frac{\left[(vt/2)^2-(x-\xi)^2\right]\left[(vt/2)^2-h^2\right]}{(vt/2)^2} \tag{7}$$

$$\sin^2\gamma = \frac{h^2\left[(vt/2)^2-(x-\xi)^2\right]}{(vt/2)^4-h^2(x-\xi)^2} \tag{8}$$

$$\cos^2\alpha = \frac{(vt/2)^2\left[(vt/2)^2-(x-\xi)^2\right]}{(vt/2)^4-h^2(x-\xi)^2} \tag{9}$$

The inverse transformation (7-9) can be found by formally solving system (4-6).

The lines of constant reflection angle γ and variable dip angle α for a given position of a reflection (diffraction) point $\{z,\xi\}$ have the meaning of summation curves for angle-gather Kirchhoff migration. The whole range of such curves for all possible values of γ covers the diffraction traveltime surface - "Cheops' pyramid" (Claerbout, 1985) in the $\{t,x,h\}$ space of seismic reflection data. As pointed out by Fowler (1997), this condition is sufficient for proving the kinematic validity of the angle-gather approach.

For comparison, Figure 2 shows the diffraction traveltime pyramid from a diffractor at 0.5 km depth. The pyramid is composed of common-offset summation curves of the conventional time migration. Figure 3 shows the same pyramid composed of constant-γ curves of the angle-gather migration.

Figure 2: Traveltime pyramid, composed of common-offset summation curves. coffset [CR]

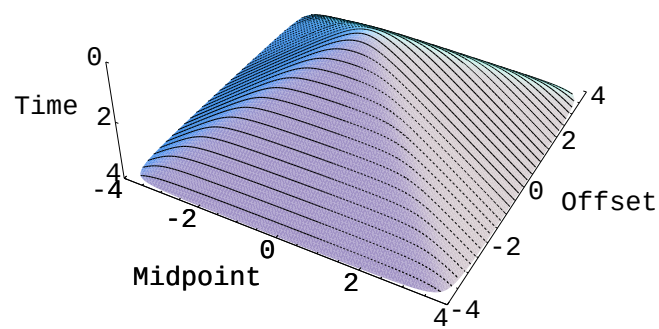

The most straightforward Kirchhoff algorithm of angle-gather migration can be formulated as follows:

- For each reflection angle γ and each dip angle α,
  - For each output location $\{z, \xi\}$,

Figure 3: Traveltime pyramid, composed of common-reflection-angle summation curves. cangle [CR]

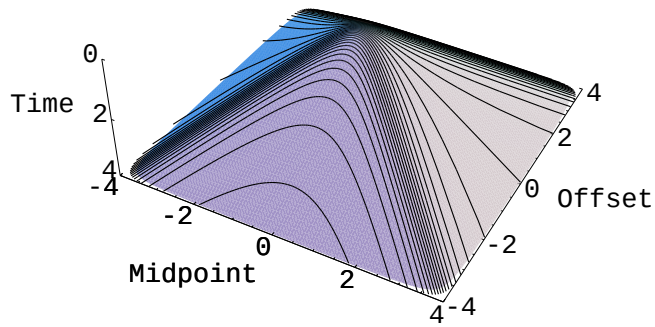

1. Find the traveltime t, half-offset h, and midpoint x from formulas (4), (5), and (6) respectively.
2. Stack the input data values into the output.

As follows from equations (4-6), the range of possible α's should satisfy the condition

$$\cos^2\alpha > \sin^2\gamma \quad \text{or} \quad |\alpha| + |\gamma| < \frac{\pi}{2}\,. \tag{10}$$

The described algorithm is not the most optimal in terms of the input/output organization, but it can serve as a basic implementation of the angle-gather

idea. The stacking step requires an appropriate weighting. We discuss the weighting issues in the next section.

3. Amplitude considerations

One simple approach to amplitude weighting for angle-gather migration is based again on Cheops' pyramid considerations. Stacking along the pyramid in the data space is a double integration in midpoint and offset coordinates. Angle-gather migration implies the change of coordinates from $\{x,h\}$ to $\{\alpha,\gamma\}$. The change of coordinates leads to weighting the integrand by the following Jacobian transformation:

$$dx\,dh = \left|\det\begin{pmatrix} \frac{\partial x}{\partial \alpha} & \frac{\partial x}{\partial \gamma} \\ \frac{\partial h}{\partial \alpha} & \frac{\partial h}{\partial \gamma} \end{pmatrix}\right| d\alpha\,d\gamma \tag{11}$$

Substituting formulas (5) and (6) into equation (11) gives us the following analytical expression for the Jacobian weighting:

$$W_{\mathrm{J}} = \left| \det \begin{pmatrix} \frac{\partial x}{\partial \alpha} & \frac{\partial x}{\partial \gamma} \\ \frac{\partial h}{\partial \alpha} & \frac{\partial h}{\partial \gamma} \end{pmatrix} \right| = \frac{z^2}{\left(\cos\alpha^2 - \sin\gamma^2\right)^2} \tag{12}$$

Weighting (12) should be applied in addition to the weighting used in common-offset migration. By analyzing formula (12), we can see that the weight increases with the reflector depth and peaks where the angles α and γ approach condition (10).

The Jacobian weighting approach, however, does not provide physically meaningful amplitudes, when migrated angle gathers are considered individually. In order to obtain a physically meaningful amplitude, we can turn to the asymptotic theory of true-amplitude migration (Goldin, 1992; Schleicher et al., 1993; Tygel et al., 1994). The true-amplitude weighting provides an asymptotic high-frequency amplitude proportional to the reflection coefficient, with the wave propagation (geometric spreading) effects removed. The generic true-amplitude weighting formula (Fomel, 1996b)

transforms in the case of 2-D angle-gather time migration to the form:

$$W_{\rm TA} = \frac{1}{\sqrt{2\,\pi}}\,\frac{\sqrt{L_s\,L_r}}{v\,\cos\gamma}\,\left|\frac{\partial^2 L_s}{\partial\xi\,\partial\gamma}+\frac{\partial^2 L_r}{\partial\xi\,\partial\gamma}\right|\,, \tag{13}$$

where L_s and L_r are the ray lengths from the reflector point to the source and the receiver respectively. After some heavy algebra, the true-amplitude expression takes the form

$$W_{\rm TA} = \frac{2\,z\,\sin\alpha}{\sqrt{2\,\pi}\,v}\,\frac{\cos^2\alpha+\sin^2\gamma}{\left(\cos^2\alpha-\sin^2\gamma\right)^{5/2}}\,. \tag{14}$$

Under the constant-velocity assumption and in high-frequency asymptotic, this weighting produces an output, proportional to the reflection coefficient, when applied for creating an angle gather with the reflection angle γ. Despite the strong assumptions behind this approach, it might be useful in practice for post-migration amplitude-versus-angle studies. Unlike the conventional common-offset migration, the angle-gather approach produces the output directly in reflection angle coordinates. One can use the generic true-amplitude theory (Fomel, 1996b) for extending formula (14) to the 3-D and

2.5-D cases.

4. Examples

We created some simple synthetic models with constant velocity backgrounds to test our angle-gather migration method. One model is a simple dome (Figure 4). The other has a series of flat reflectors of various dips (Figure 5). Both of these figures also show the corresponding data that will be generated by Kirchhoff methods for zero and far offsets.

4.1. Dome model

This model contains a wide range of geologic dips across the dome as well as having a flat reflector at the base of the dome. Figure 6 shows the resulting common offset sections from traditional Kirchhoff migration. As is expected for such a simple model, the near and far offset sections are very similar and the stacked section is almost perfect. We are more interested in the result of the angle-gather migration.

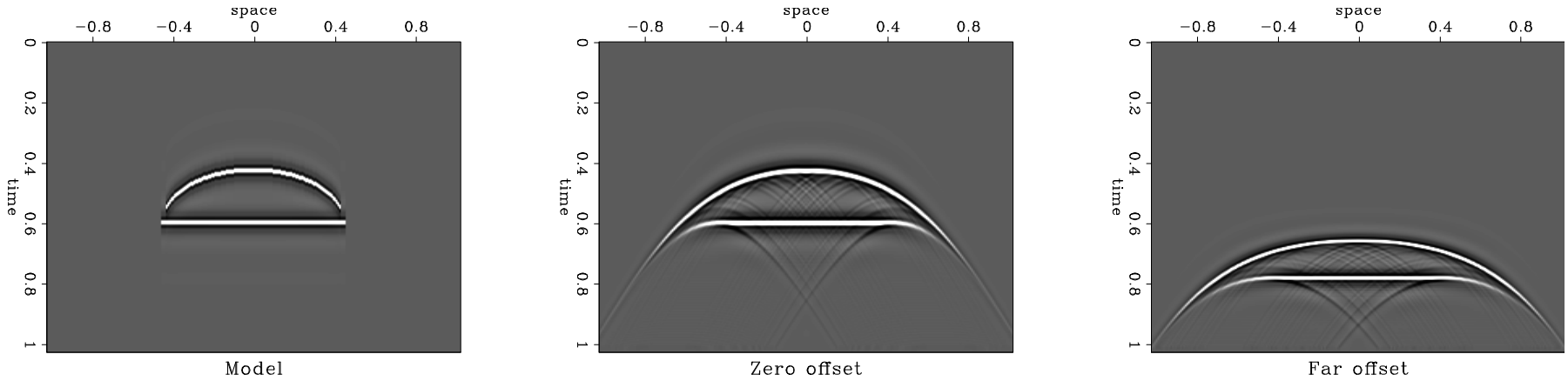

Figure 4: Left: Model. Center: Data at zero offset. Right: Data at far offset. data.dome [ER]

Figure 7 shows the zero and large angle sections as well as the stack for angle-gather Kirchhoff migration. The zero-angle section is weak but clearly shows the correct shape and position. The large-angle section is actually only for $\gamma = 25°$. The reason for this is clear if you consider Figure 1. At greater depths, the rays associated with large reflection angles (γ) will not emerge at the surface within the model space. Therefore at angles greater than 25° (the maximum useful angle), the information at later times

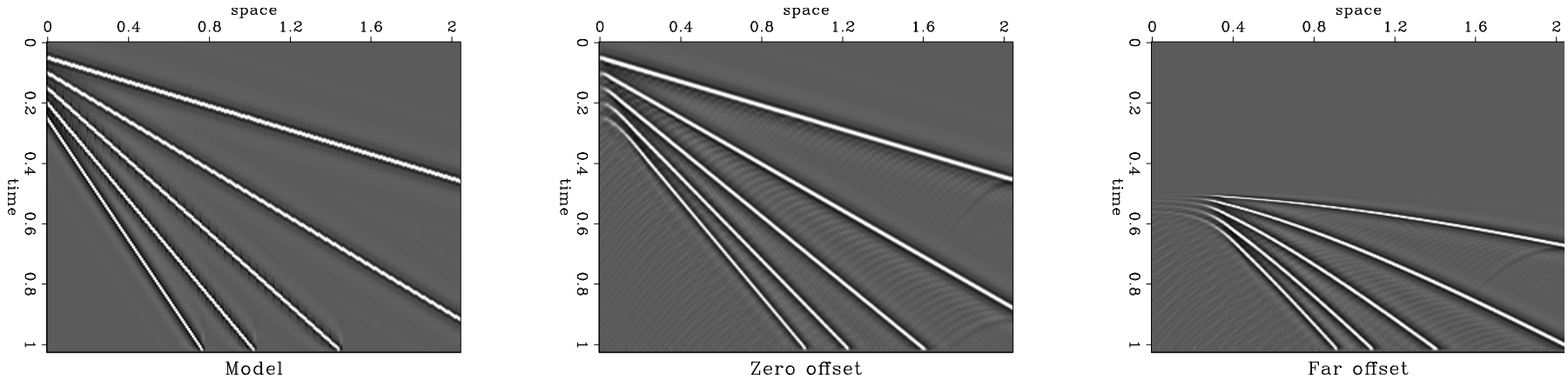

Figure 5: Left: Model. Center: Data at zero offset. Right: Data at far offset. data.lines [ER]

disappears.

We expect the stacked sections for the offset method and the angle method to be identical. Although we sum over different paths for the offset-domain migration (Figure 2) and the angle-domain migration (Figure 3), the stack should sum all of the same information together for both methods. Fortunately, a comparison of the stacked sections in Figures 6 and 7 show that the results are identical as expected.

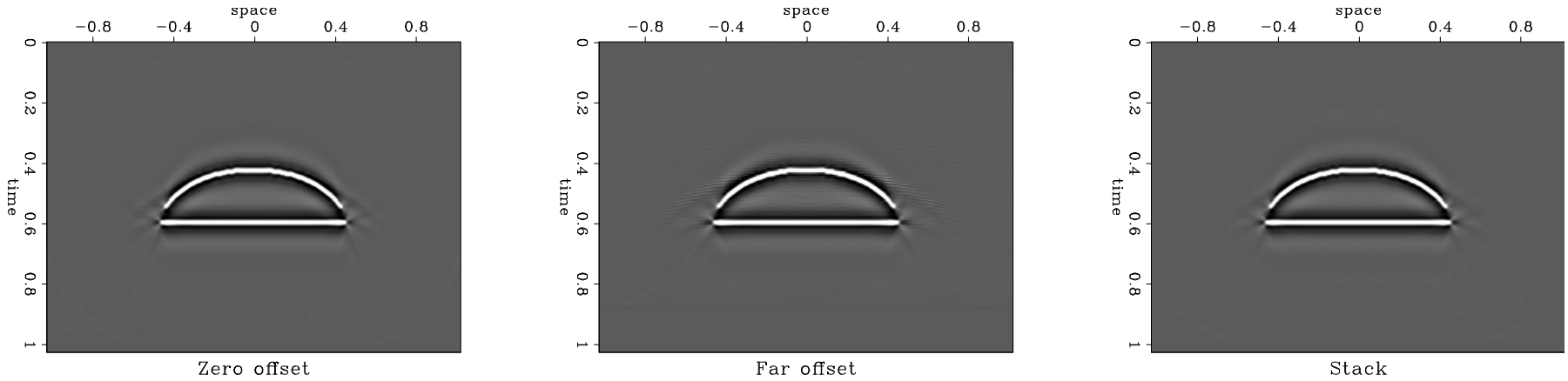

Figure 6: Left: Migrated offset section at zero offset. Center: Migrated offset section at far offset. Right: Stack. offset.dome [ER]

4.2. Dipping reflectors model

This model contains fewer dips than the dome model but it allows us to see what is happening at later times. Figure 8 shows the common offset sections and stacked section from offset-domain Kirchhoff migration. Once again, they are practically perfect. The only problem is near the bottom of the section where we lose energy because the data was truncated.

The zero-angle and large-angle sections from the angle-domain migra-

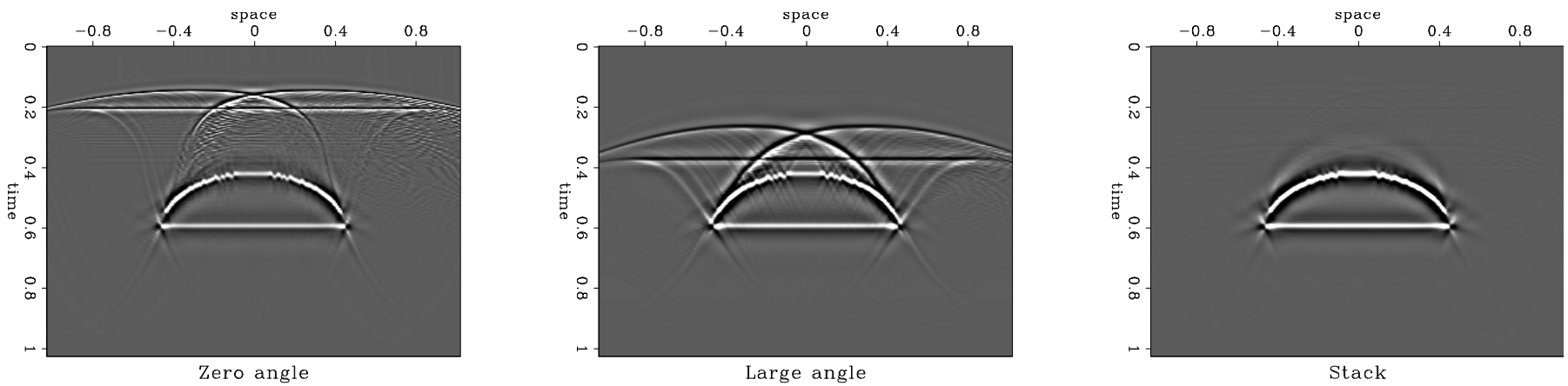

Figure 7: Left: Migrated angle section at small angle. Center: Migrated offset section at large angle. Right: Stack. angle-ta.dome [ER]

tion are in Figure 9, along with the stacked section. Once again, the zero angle section is very weak and the large angle section only contains information down to a time of $\approx$ .85 seconds, for the same reason as explained for the dome model.

Once again, we expect the stacked sections in Figures 8 and 9 to be the same. Although the angle-domain stack is slightly lower amplitude throughout the section, it is clear that this is a simple scale factor so our expectations remain intact.

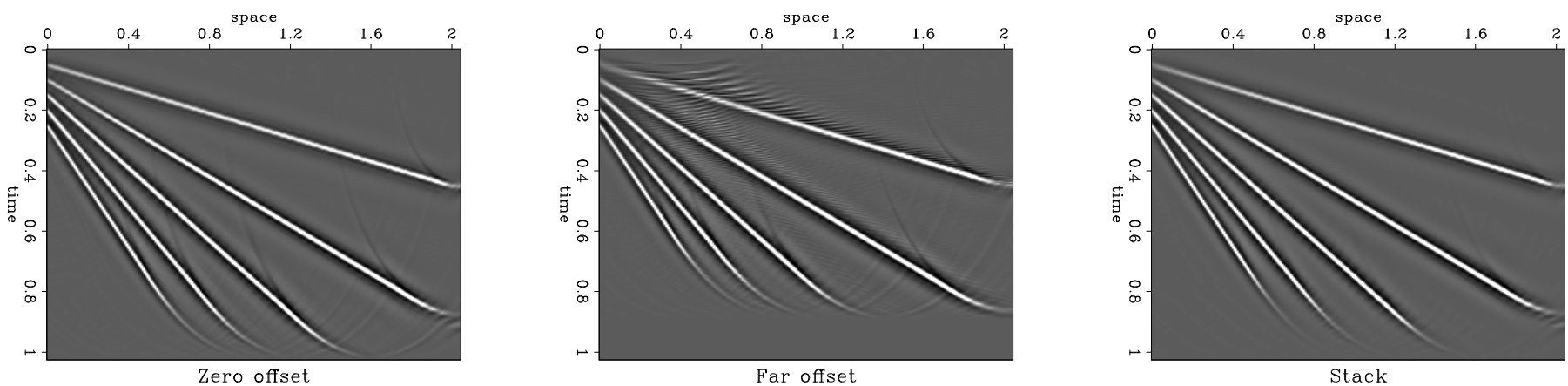

Figure 8: Left: Migrated offset section at zero offset. Center: Migrated offset section at far offset. Right: Stack. offset.lines [ER]

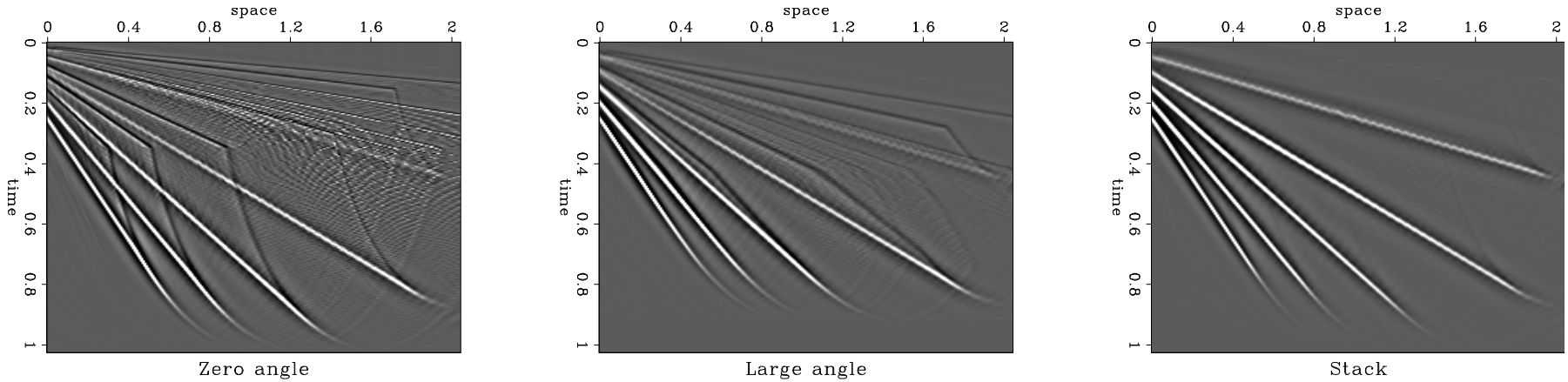

Figure 9: Left: Migrated angle section at zero angle. Center: Migrated angle section at large angle. Right: Stack. angle-ta.lines [ER]

4.3. Reflectivity variation with angle

Amplitude variation with offset (AVO) would not be expected to be very interesting for the simple models just shown. Consider Figure 10 which contains an offset gather and a reflection angle gather taken from space location zero from the dome model in Figure 4. The offset gather shows exactly what we expect for such a model - no variation. The angle gather also shows no

variation for angles less than the maximum useful angle (25°) as discussed in the previous two subsections. However, when the angle exceeds the maximum useful angle, the event increases in amplitude and width. This is the phenomenon seen in de Bruin et al. (1990).

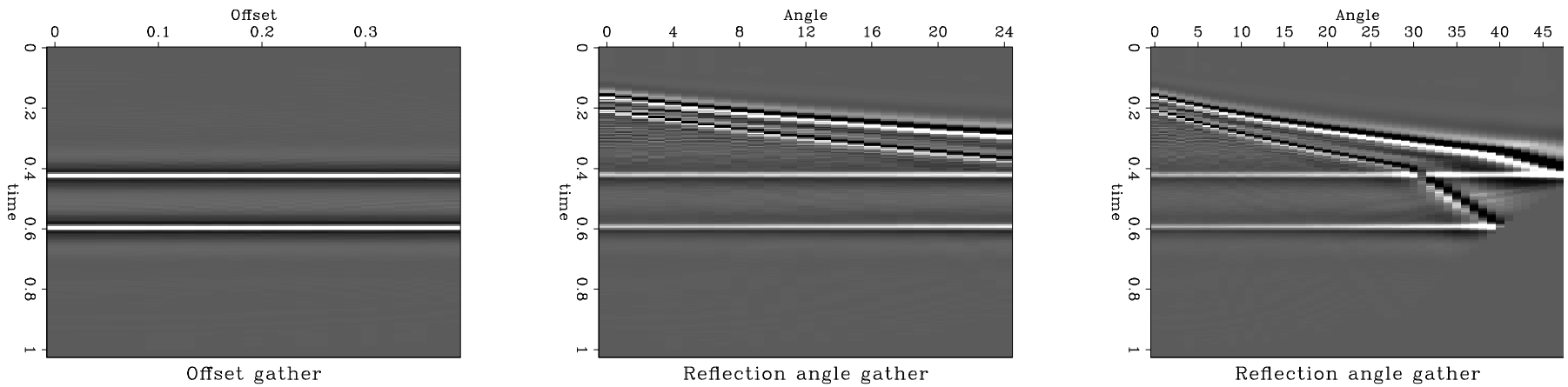

Figure 10: Gathers taken from space location zero in the dome model. Left: Offset domain. Center: Angle domain less than 25°. Right: Angle domain. reflect-ta.dome [ER]

4.4. Velocity sensitivity

When dealing with real data we almost never know what the true velocity of the subsurface is. Therefore it is important to understand the effects of velocity on our angle-gather time migration algorithm. To do this we simply created data for the dome model in Figure 4 at a fairly high velocity (3 km/s) and migrated it using a low velocity (1.5 km/s). The results are in Figure 11. For angles less than the maximum useful angle ($\gamma = 25°$), the angle-domain gather behaves exactly as the offset-domain gather does. Beyond the maximum useful angle, the events become even more curved and the amplitudes begin to change.

The behavior of the angle-gather migration is very similar to that of offset-domain migration as long as the limitation of the maximum useful angle is recognized. Therefore, we can probably expect angle-gather migration to behave like offset-domain migration in $v(z)$ media also.

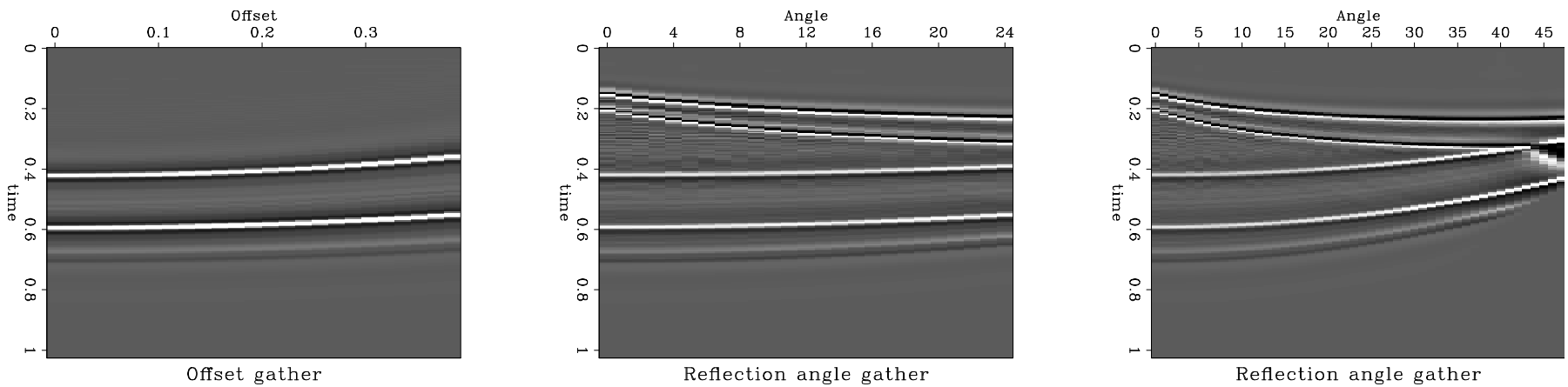

Figure 11: Gathers taken from space location zero inthe dome model and migrated at too low a velocity. Left: Offset domain. Center: Angle domain less than 25°. Right: Angle domain. reflect-ta.fast.dome [ER]

5. Frequency-domain considerations

As pointed out by Prucha et al. (1999), the angle gathers can be conveniently formed in the frequency domain. This conclusion follows from the simple formula (Fomel, 1996a)

$$\tan\gamma = \frac{\partial z}{\partial h}\ , \tag{15}$$

where z refers to the depth coordinate of the migrated image. In the frequency-wavenumber domain, formula (15) takes the trivial form

$$\tan\gamma = \frac{k_h}{k_z}\ . \tag{16}$$

It indicates that angle gathers can be conveniently formed with the help of frequency-domain migration algorithms (Stolt, 1978). This interesting opportunity requires further research.

6. Conclusions

We have presented an approach to time migration based on angle gathers. The output of this procedure are migrated angle gathers - images for constant reflection angles. When stacked together, angle gathers can produce the same output as the conventional common-offset gathers. Looking at angle gathers individually opens new possibilities for amplitude-versus-angle studies and for velocity analysis.

Our first synthetic tests produced promising results. In the future, we plan to study the amplitude behavior of angle-gather migration and the velocity sensitivity more carefully. We also plan to investigate the frequency-domain approaches to this method. Initial results indicate that angle-gather migration is comparable to offset-domain migration for angles less than the angle at which rays exit the sides of the model, but further study will hopefully allow us to extract useful information from the larger angles as well. Although the major advantages of angle gathers lay in the depth migration domain, it is easier to analyze the time migration results because of their theoretical simplicity.

7. REFERENCES

Claerbout, J. F., 1985, Imaging the Earth's Interior: Blackwell Scientific Publications. 6

de Bruin, C., Wapenaar, C., and Berkhout, A., 1990, Angle-dependent reflectivity by means of prestack migration: Geophysics, **55**, no. 9, 1223–1234. 19

Fomel, S., 1995, Amplitude preserving offset continuation in theory Part 1: The offset continuation equation: SEP–**84**, 179–198. 4

Fomel, S., 1996a, Migration and velocity analysis by velocity continuation: SEP–**92**, 159–188. 4, 22

Fomel, S., 1996b, Stacking operators: Adjoint versus asymptotic inverse: SEP–**92**, 267–292. 10, 11

Fomel, S., 1997, Velocity continuation and the anatomy of residual prestack

migration: 67th Ann. Internat. Meeting, Soc. Expl. Geophys., Expanded Abstracts, 1762–1765. 4

Fowler, P., 1997, A comparative overview of prestack time migration methods: 67th Annual Internat. Mtg., Soc. Expl. Geophys., Expanded Abstracts, 1571–1574. 3, 6

Goldin, S. V., 1992, Estimation of reflection coefficient under migration of converted and monotype waves: Soviet Geology and Geophysics, **33**, no. 4, 76–90. 10

Prucha, M. L., Biondi, B. L., and Symes, W. W., 1999, Angle-domain common image gathers by wave-equation migration: SEP–**100**, 101–112. 2, 22

Schleicher, J., Tygel, M., and Hubral, P., 1993, 3-D true-amplitude finite-offset migration: Geophysics, **58**, no. 8, 1112–1126. 10

Stolt, R. H., 1978, Migration by Fourier transform: Geophysics, **43**, no. 1, 23–48. 22

Tygel, M., Schleicher, J., and Hubral, P., 1994, Kirchhoff-Helmholtz theory in modeling and migration: Journal of Seismic Exploration, **3**, 203–214. 10